

# Overtone spectroscopy of H<sub>2</sub>O clusters in the $\nu_{\text{OH}}=2$ manifold: Infrared-ultraviolet vibrationally mediated dissociation studies

Sergey A. Nizkorodov,<sup>a)</sup> Michael Ziemkiewicz, and David J. Nesbitt<sup>b)</sup>  
*JILA, University of Colorado, Boulder, Colorado 80309; National Institute of Standards and Technology, Boulder, Colorado 80309; and Department of Chemistry and Biochemistry, University of Colorado, Boulder, Colorado 80309*

Alan E. W. Knight  
*Faculty of Science and Technology, Griffith University, Nathan Campus, Brisbane, Queensland 4111, Australia*

(Received 24 September 2004; accepted 8 March 2005; published online 18 May 2005)

Spectroscopy and predissociation dynamics of (H<sub>2</sub>O)<sub>2</sub> and Ar–H<sub>2</sub>O are investigated with vibrationally mediated dissociation (VMD) techniques, wherein  $\nu_{\text{OH}}=2$  overtones of the complexes are selectively prepared with direct infrared pumping, followed by 193 nm photolysis of the excited H<sub>2</sub>O molecules. As a function of relative laser timing, the photolysis breaks H<sub>2</sub>O into OH and H fragments either (i) directly inside the complex or (ii) after the complex undergoes vibrational predissociation, with the nascent quantum state distribution of the OH photofragment probed via laser-induced fluorescence. This capability provides the first rotationally resolved spectroscopic analysis of (H<sub>2</sub>O)<sub>2</sub> in the first overtone region and vibrational predissociation dynamics of water dimer and Ar–water clusters. The sensitivity of the VMD approach permits several  $\nu_{\text{OH}}=2$  overtone bands to be observed, the spectroscopic assignment of which is discussed in the context of recent anharmonic theoretical calculations. © 2005 American Institute of Physics.  
[DOI: 10.1063/1.1899157]

## I. INTRODUCTION

Water dimer, (H<sub>2</sub>O)<sub>2</sub>, is arguably one of the most important binary complexes in nature. It has been intensively studied ever since its first spectroscopic observation in a solid nitrogen matrix<sup>1</sup> and in gas phase.<sup>2,3</sup> The most significant spectroscopic studies of (H<sub>2</sub>O)<sub>2</sub> include a comprehensive symmetry classification of its tunneling-rotational energy levels,<sup>4</sup> observation of low-resolution infrared,<sup>5–7</sup> and coherent anti-Stokes Raman scattering<sup>8</sup> spectra of jet-cooled water complexes as well as observation of high-resolution infrared,<sup>9–12</sup> far-infrared,<sup>13–15</sup> cavity ring down,<sup>12</sup> and microwave<sup>16,17</sup> spectra of water dimer. This, in turn, has led to determination of a reliable water pair potential<sup>18–20</sup> and elegant infrared spectra of size-selected water clusters,<sup>21</sup> resolving many discrepancies in previous spectroscopic assignment of (H<sub>2</sub>O)<sub>2</sub> fundamental transitions.

In spite of the impressive roster of spectroscopic studies of (H<sub>2</sub>O)<sub>2</sub> and larger water clusters, relatively little is known about their OH stretching overtones. Overtone excitations in (H<sub>2</sub>O)<sub>2</sub> are especially interesting because of their potential effect on the dynamics of donor-acceptor switching and other hydrogen bond tunneling-interchange motions in the complex. There have been just a few theoretical studies of the positions and transition strengths of (H<sub>2</sub>O)<sub>n</sub> overtone bands.<sup>22–25</sup> Matrix isolation vibrational spectra of H<sub>2</sub>O poly-

mers in the OH-overtone range have been reported only recently.<sup>26,27</sup> No gas-phase spectra of (H<sub>2</sub>O)<sub>2</sub> overtone bands are presently available.

Additional interest in the overtone spectroscopy of (H<sub>2</sub>O)<sub>2</sub> stems from the potential atmospheric importance of water clusters.<sup>19,28,29</sup> Atmospheric (H<sub>2</sub>O)<sub>2</sub> influences the radiation balance of the planet,<sup>28</sup> homogeneous nucleation dynamics of aerosol formation,<sup>30</sup> and even rates and mechanisms of certain chemical reactions.<sup>31–34</sup> Overtone spectroscopy is a powerful potential tool for quantitative characterization of (H<sub>2</sub>O)<sub>2</sub> column abundances in the atmosphere. Indeed, a weak band at 749.5 nm recently detected<sup>35</sup> in long-pass atmospheric spectra has been tentatively assigned to the bound OH ( $\nu_{\text{OH}}=4$ ) third overtone transition of (H<sub>2</sub>O)<sub>2</sub> based on comparison with the existing theoretical predictions.<sup>24,25</sup> Lower order overtones of (H<sub>2</sub>O)<sub>2</sub>, such as  $\nu_{\text{OH}}=2$  bands described here, may be more convenient for observational work on atmospheric (H<sub>2</sub>O)<sub>2</sub> because of their less ambiguous spectroscopic assignments.

This manuscript examines  $\nu_{\text{OH}}=2$  vibrational states of (H<sub>2</sub>O)<sub>2</sub> using an approach of vibrationally mediated dissociation,<sup>36–40</sup> wherein selectively prepared rovibrational states of H<sub>2</sub>O complexes are photolyzed and the resulting OH photofragments are detected with full quantum state resolution (Fig. 1). This method provides detailed information not only about overtone spectroscopy, but also about molecular energy transfer dynamics in H<sub>2</sub>O and its complexes. Specifically, this paper presents the first observation of the  $\nu_{\text{OH}}=2$  overtones in (H<sub>2</sub>O)<sub>2</sub> with partial rotational

<sup>a)</sup>Present address: Department of Chemistry, University of California, Irvine, CA 92697.

<sup>b)</sup>Author to whom correspondence should be addressed; Electronic mail: djn@jila.colorado.edu

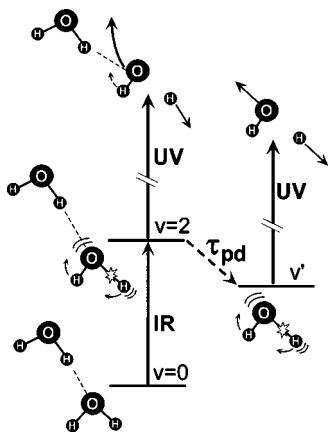


FIG. 1. Experimental approach. Complexes are excited in  $v_{\text{OH}}=2$  state followed by photodissociation of  $\text{H}_2\text{O}(v_{\text{OH}}=2)$  directly inside the complexes with a UV laser pulse (left). Alternatively, the excited complexes first predissociate on time scale  $\tau_{pd}$  generating  $\text{H}_2\text{O}$  molecules in a different vibrational state ( $v'$ ), which are then photodissociated by the photolysis laser (right). In either case, the resulting OH fragments are detected in specific final quantum states by laser-induced fluorescence.

resolution and provides information about the dynamics of  $(\text{H}_2\text{O})_2$  predissociation at the  $v_{\text{OH}}=2$  excitation energies ( $\approx 7000\text{ cm}^{-1}$ ).

By way of contrast, the much simpler complex between Ar and  $\text{H}_2\text{O}$  provides a useful juxtaposition with  $(\text{H}_2\text{O})_2$ .<sup>40,41</sup> Compared to the water dimer, Ar- $\text{H}_2\text{O}$  has a substantially smaller potential energy well depth [ $140\text{ cm}^{-1}$  in Ar- $\text{H}_2\text{O}$  vs  $1700\text{ cm}^{-1}$  in  $(\text{H}_2\text{O})_2$ ] (Refs. 18 and 42) and considerably weaker interactions between intermolecular and intramolecular modes. This makes Ar- $\text{H}_2\text{O}$  a convenient system for studying photodissociation dynamics of  $\text{H}_2\text{O}$  in the presence of a weakly perturbing rare gas “solvent” as opposed to the strongly hydrogen-bonded interactions present in  $(\text{H}_2\text{O})_2$ . Vibrationally mediated dissociation studies of Ar- $\text{H}_2\text{O}$  in the  $v_{\text{OH}}=3$  manifold have been reported<sup>40</sup> but none in the first overtone region corresponding to the present study of  $\text{H}_2\text{O}$  dimer. To establish a suitable experimental perspective for the more complicated spectra of  $(\text{H}_2\text{O})_2$ , this study therefore also briefly considers vibrationally mediated spectroscopy and dynamics out of selected  $v_{\text{OH}}=2$  vibrational states of Ar- $\text{H}_2\text{O}$ .

## II. EXPERIMENT

Pertinent experimental information has been summarized in recent work dealing with the dynamics of vibrationally mediated dissociation of  $\text{H}_2\text{O}$  monomer in the  $v_{\text{OH}}=2$  polyad;<sup>43</sup> thus only the most relevant details are summarized here. Ar- $\text{H}_2\text{O}$  and  $(\text{H}_2\text{O})_2$  complexes are produced in a supersonic expansion of 1%  $\text{H}_2\text{O}$  in 30% Ar/70% He mixture through a pulsed slit valve ( $4\text{ cm} \times 125\ \mu\text{m}$ , 10 Hz, 0.5 ms). The best yields of Ar- $\text{H}_2\text{O}$  and  $(\text{H}_2\text{O})_2$  complexes are achieved at a total stagnation pressure of 300–500 Torr, with the yield of dimer decreasing at higher pressures or at larger Ar fractions presumably because of preferential formation of larger clusters. The  $v_{\text{OH}}=2$  overtone vibrations of jet-cooled molecules are excited with a tunable near-infrared pump laser ( $\nu=7100\text{ cm}^{-1}$ – $7300\text{ cm}^{-1}$ , up to

20–30 mJ/pulse,  $0.2\text{ cm}^{-1}$  resolution, 5 ns pulse width). A counterpropagating ArF excimer photolysis laser pulse (193 nm, 5 mJ/pulse, 7 ns pulse width) follows after a variable time delay (0–1000 ns) with respect to the pump, dissociating a fraction of vibrationally excited water molecules (Fig. 1). Finally, a probe laser pulse ( $30\ \mu\text{J}$ /pulse,  $0.1\text{ cm}^{-1}$ , 5 ns) excites the nascent OH on the off-diagonal  $A^2\Sigma \leftarrow X^2\Pi\ v=1 \leftarrow 0$  band some 20 ns after the photolysis pulse, with the resulting OH fluorescence collected from the diagonal  $A^2\Sigma \leftarrow X^2\Pi\ v=1 \leftarrow 0$  band at 310 nm. Both excitation and detection take place  $\approx 2\text{ cm}$  downstream from the expansion slit. To discriminate between (i) vibrationally mediated and (ii) direct 193 nm photolysis of  $\text{H}_2\text{O}$  and its complexes, the near-infrared pump laser is operated at half the repetition rate, with the data from alternate laser shots subtracted to generate a background-free signal.

The resulting OH fluorescence signal is found to be linear in the 193 nm photolysis laser power, indicating that multiphoton photodissociation processes in the parent molecule are not relevant. The OH transitions are then probed in the weak saturation limit and calibrated against fluorescence excitation spectra under fully thermalized conditions. On the other hand, the IR pump transitions can be saturated significantly, despite the decrease in absorption strength with successive overtone excitation. Indeed, for the strongest overtone transitions, it proves necessary to attenuate the pump laser power by as much as two orders of magnitude to avoid power-broadening of spectral lines beyond the specified laser resolution of  $0.2\text{ cm}^{-1}$ . For optimal sensitivity, therefore, overview scans are taken under full near-IR pump laser power, with scans of individual overtone bands taken under reduced power conditions.

## III. RESULTS AND DISCUSSION

### A. Spectroscopic notation

We use  $|mn\rangle^\pm$  local mode notation<sup>44</sup> for labeling OH-stretching vibrations of free  $\text{H}_2\text{O}$ , Ar- $\text{H}_2\text{O}$ , and the monomer proton acceptor subunit in  $(\text{H}_2\text{O})_2$ , where  $m$  and  $n$  are the local mode-stretching quanta.<sup>45</sup> In this notation, one can approximately correlate  $\nu_1 + \nu_3$  and  $2\nu_1$  normal mode states of  $\text{H}_2\text{O}$  with  $|02\rangle^-$  and  $|02\rangle^+$  local mode states, respectively. For the proton-donor unit of  $(\text{H}_2\text{O})_2$ , the states are labeled by specifying the number of local mode excitations in the bound-OH and free-OH bonds.<sup>24</sup> For example,  $|0\rangle_f|1\rangle_b$  designates the  $v_{\text{OH}}=1$  hydrogen-bonded OH stretch fundamental vibration of  $(\text{H}_2\text{O})_2$ .

We use the notation of Ref. 10 for labeling rotational states of  $(\text{H}_2\text{O})_2$ . Briefly, each rotational level of  $(\text{H}_2\text{O})_2$  is split into sextets by three internal motions: acceptor internal rotation, acceptor-donor interchange, and donor proton interchange (Fig. 2). Internal rotation of the proton acceptor subunit is extremely facile, splitting each  $J, K$  state into widely separated “upper” and “lower”  $K$  manifolds (e.g.,  $\approx 10\text{ cm}^{-1}$  between  $K_{\text{lower}}=0$  and  $K_{\text{upper}}=0$ ), with acceptor-donor interchange and donor switching resulting in more modest additional splittings of each  $K$  level into  $A_{1,2}$ ,  $E$ , and  $B_{1,2}$  sublevels (e.g.,  $A_2^-$  and  $B_2^-$  are separated by  $\approx 0.65\text{ cm}^{-1}$  in  $J=0$ ,  $K_{\text{upper}}=0$ ). Furthermore, all  $K \neq 0$  levels are split into dou-

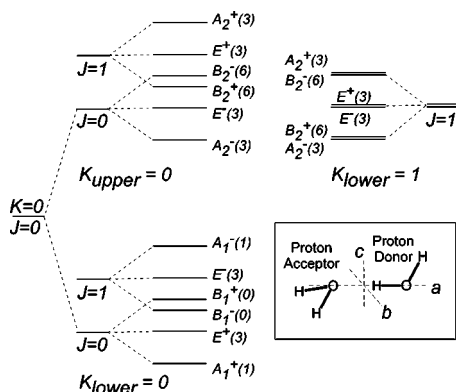


FIG. 2. Schematic diagram of (H<sub>2</sub>O)<sub>2</sub> energy levels (not to scale) and principal inertial axes for (H<sub>2</sub>O)<sub>2</sub>. Only  $K$  levels appreciably populated at jet temperatures are shown. Each  $K$  level is split into  $K_{\text{lower}}$  and  $K_{\text{upper}}$  components by proton acceptor internal rotation. Further splitting arises because of donor-acceptor interchange. For  $K > 0$ , there is an additional doubling of all levels. The total symmetry including rotation (in permutation-inversion group isomorphic to  $D_{4h}$ ) and nuclear weights for each level are given for a totally symmetric vibration of (H<sub>2</sub>O)<sub>2</sub>.

plets by conventional asymmetry considerations. The  $K_{\text{lower}} = 1$  and  $K_{\text{upper}} = 0$  manifolds are close in energy because of the comparable tunneling and  $K_a = 1$  rotational pathways around the  $A$  axis. Finally, (H<sub>2</sub>O)<sub>2</sub> molecules under supersonic conditions cool down to the lowest levels within its five nuclear spin symmetry subgroups ( $A_1$ ,  $E$ ,  $B_1$ ,  $A_2$ , and  $B_2$ ) with a fairly large spacing (10 cm<sup>-1</sup>) between the  $A_1$ ,  $E$ ,  $B_1$  and  $A_2$ ,  $B_2$  manifolds. To the extent that all internal motion in H<sub>2</sub>O dimer is maximally cooled, one would quite simply expect comparable ( $\approx 7:9$ ) populations in the  $K_{\text{lower}} = 0$  vs  $K_{\text{upper}} = 0 / K_{\text{lower}} = 1$  manifolds.

The energy levels of Ar-H<sub>2</sub>O are much more simply represented in the framework of nearly freely rotating H<sub>2</sub>O in the slightly anisotropic potential resulting from the Ar atom. Specifically, *ortho* and *para* nuclear spin designations are still good, and the energy levels of the complex can be conveniently labeled by quantum numbers of the free H<sub>2</sub>O rotational states ( $J_{K_a K_c}$ ) with which they correlate. Ar-H<sub>2</sub>O levels are additionally characterized by the projection of the total angular momentum on the intermolecular axis and by the number of quanta in the intermolecular stretching mode  $\nu_s$ , as explained in Refs. 46 and 47. Figure 3 displays a schematic diagram of the lowest energy levels of Ar-H<sub>2</sub>O adopted from far-infrared and near-infrared studies<sup>11,42,47,48</sup> along with allowed transitions for  $|02\rangle^-$  band.

## B. Overview spectrum

Figure 4 shows an overview spectrum recorded under conditions optimized for the maximal yield of Ar-H<sub>2</sub>O complexes. The spectrum is obtained by tuning the UV probe laser on the  $Q_{11}(8)$  line of the  $A^2\Sigma \leftarrow X^2\Pi$   $v=1 \leftarrow 0$  band that probes the  $^2\Pi_{3/2} N=8$  rotational state of OH ( $v=0$ ) and then continuously scanning the near-infrared pump laser frequency over the characteristic first OH-stretching overtone region. As will be elucidated below, the choice of a relatively high- $N$  state of OH for detection (e.g.,  $N=8$  vs  $N=1$ ) is used to maximize action spectral intensities from complexes relative to those from H<sub>2</sub>O monomer. In addition to a strong

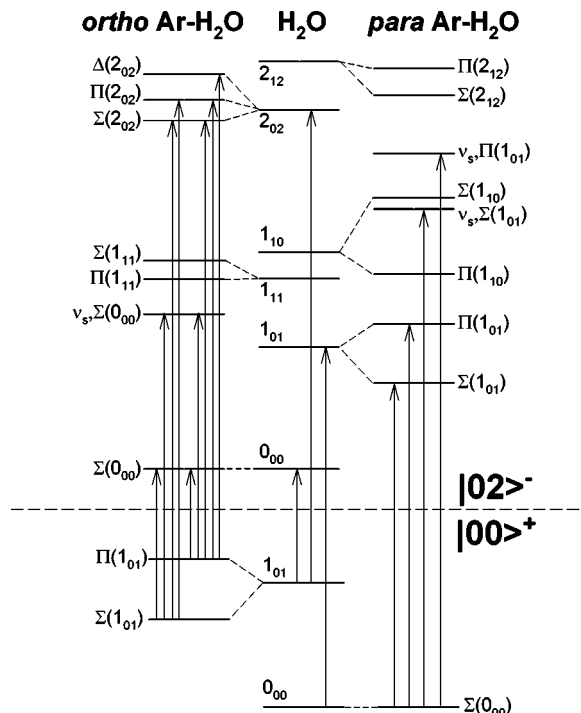


FIG. 3. Correlation between the Ar-H<sub>2</sub>O and H<sub>2</sub>O energy levels. The grid of the Ar-H<sub>2</sub>O levels is shifted with respect to that of H<sub>2</sub>O by the binding energy of the complex. For  $|02\rangle^-$  vibrational state, the *ortho* and *para* labels are interchanged compared to  $|00\rangle^+$  on the account of the asymmetry of the vibration, with the  $|02\rangle^- \leftarrow |00\rangle^+$  transitions following  $a$ -type selection rules:  $\Delta K_a = \text{even}$ ,  $\Delta K_c = \text{odd}$ .

dependence on OH probe state, band intensities in the spectrum are also affected by time delay between the pump and photolysis laser pulses, because vibrationally excited complexes can undergo intermolecular predissociation *before* H<sub>2</sub>O molecules inside them are photolyzed (Fig. 1). Indeed, this will serve as a basis for direct measurement of vibrational predissociation lifetimes for Ar-H<sub>2</sub>O and (H<sub>2</sub>O)<sub>2</sub>, as described later. The spectra in Fig. 4 are obtained with a pump-photolysis delay chosen to be 500 ns; this effectively ensures that all complexes predissociate prior to photolysis by the excimer laser pulse.

As the first stage in the spectral assignment, only three rovibrational transitions of jet-cooled H<sub>2</sub>O appear in this spectral range and with appreciable intensity; these correspond to  $J_{K_a K_c} = 1_{01} \leftarrow 0_{00}$  (*para*) and  $0_{00} \leftarrow 1_{01}$  and  $2_{02} \leftarrow 1_{01}$  (*ortho*) transitions in the  $|02\rangle^-$  vibrational overtone band. A few H<sub>2</sub>O monomer transitions into  $|02\rangle^+$  state also occur in this spectral range but are considerably weaker and indeed undetectable at the current  $S/N$  in Fig. 4. The remaining bands in the spectrum cannot be attributed to free H<sub>2</sub>O lines and, therefore, must belong to complexes containing H<sub>2</sub>O. Note that these bands are of comparable intensity to vibrationally mediated water monomer lines. This is not a reflection of water clustering efficiency but rather that detection on high OH( $N$ ) states provides an enormous discrimination against water monomer, obviously present in much higher concentrations.

Many bands in the action spectrum are strongly correlated with fractional Ar content in the expansion mixture, suggesting complexes between H<sub>2</sub>O and Ar (Table I and Fig.

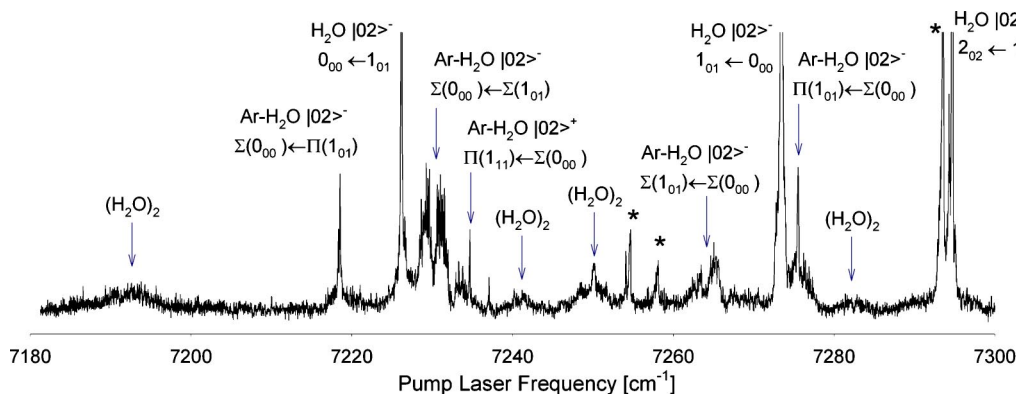


FIG. 4. Survey action spectrum. The probe laser is tuned to the  ${}^2\Pi_{3/2}$  (8) rotational state of  $\text{OH}(v=0)$ , while the pump laser is scanned in frequency. The time delay between the IR pump and UV photolysis laser is sufficiently long to allow all vibrationally excited complexes to predissociate. Apart from a few easily identifiable  $\text{H}_2\text{O}$  monomer lines, all the structure in the spectrum is due to  $\text{Ar-H}_2\text{O}$  and  $(\text{H}_2\text{O})_2$ . The bands labeled with asterisks almost certainly belong to  $\text{Ar-H}_2\text{O}$  but require further studies for definitive assignment.

4). Indeed, some of these bands display partially resolved rotational structure consistent with the  $\text{Ar-H}_2\text{O}$  binary complex. A significant number of bands in the spectrum remain even if Ar is completely replaced by He in the carrier gas mixture. However, their signal intensities are reduced because of much smaller clustering efficiency in pure He jets. Since  $\text{He-H}_2\text{O}$  clustering is expected to be negligible under room temperature stagnation conditions, these can be assigned to overtone spectra of  $(\text{H}_2\text{O})_n$  complexes (Table I). To the best of our knowledge, this represents the first such overtone spectra for neutral  $\text{H}_2\text{O}$  clusters, specifically made possible by the enhanced sensitivity of vibrationally mediated photodissociation methods. Indeed, at least one of these bands (at  $7193\text{ cm}^{-1}$ ) even exhibits partially resolved *rotational* structure characteristic of  $\text{H}_2\text{O}$  dimer, to which we next direct our attention.

### C. First overtone ( $v_{\text{OH}}=2$ ) spectra of $\text{H}_2\text{O}$ dimer

Vibrational assignment of the OH-stretching bands of  $(\text{H}_2\text{O})_2$  has historically proven to be a challenging task, even at the *fundamental* level. Indeed, the four OH-stretching fundamentals have been reassigned several times and only more

TABLE I. Positions and assignments of the observed overtone bands of  $\text{Ar-H}_2\text{O}$  and  $(\text{H}_2\text{O})_n$ . Positions are accurate to within  $0.2\text{ cm}^{-1}$ . Whereas  $\text{Ar-H}_2\text{O}$  assignments are relatively certain,  $(\text{H}_2\text{O})_2$  assignments should be considered speculative and a source of stimulation for further theoretical efforts.

Positions ( $\text{cm}^{-1}$ )	Carrier	Band shape	Assignment
7193 <sup>a</sup>	$(\text{H}_2\text{O})_2$		$ 02\rangle_a^+$ or $ 1\rangle_f 1\rangle_b$
7218.45 <sup>b</sup>	$\text{Ar-H}_2\text{O}$	⊥	$ 02\rangle^- \Sigma(0_{00}) \leftarrow \Pi(1_{01})$
7230.05 <sup>c</sup>	$\text{Ar-H}_2\text{O}$		$ 02\rangle^- \Sigma(0_{00}) \leftarrow \Sigma(1_{01})$
7240 <sup>b</sup>	$(\text{H}_2\text{O})_2$	⊥ <sup>d</sup>	Most likely $ 2\rangle_f 0\rangle_b$
7249.8 <sup>b</sup>	$(\text{H}_2\text{O})_2$	⊥ <sup>d</sup>	Most likely $ 2\rangle_f 0\rangle_b$
7263.7 <sup>a</sup>	$\text{Ar-H}_2\text{O}$		$ 02\rangle^- \Sigma(1_{01}) \leftarrow \Sigma(0_{00})$
7275.0 <sup>b</sup>	$\text{Ar-H}_2\text{O}$	⊥	$ 02\rangle^- \Pi(1_{01}) \leftarrow \Sigma(0_{00})$
7282 <sup>a</sup>	$(\text{H}_2\text{O})_2$	<sup>d</sup>	

<sup>a</sup>Approximate band center.

<sup>b</sup>Q-branch position.

<sup>c</sup>Band origin from fitting.

<sup>d</sup>Poorly defined band shape.

or less definitively understood from recent cluster size-selective spectroscopic work of Huisken *et al.*<sup>21</sup> Table II summarizes the presently accepted assignments at the  $v_{\text{OH}}=1$  level. With two quanta of OH-stretching excitation, the overtone spectral region is certain to be significantly more complex; for example, there are as many as ten different possibilities to distribute them among the four OH bonds in  $(\text{H}_2\text{O})_2$ .

Fortunately, theory predicts only a few of these combination states to be efficiently produced from the ground state of  $(\text{H}_2\text{O})_2$  via direct overtone pumping. Harmonically coupled anharmonic oscillator (HCAO) calculations by Kjaergaard and co-workers<sup>24,25</sup> predict that the strongest OH overtone transitions in  $(\text{H}_2\text{O})_2$  should be  $|02\rangle_a^+$ ,  $|2\rangle_f|0\rangle_b$ ,  $|02\rangle_a^+$ , and  $|1\rangle_f|1\rangle_b$  (listed in the order of decreasing transition strengths), where *a*, *f*, and *b* refer to proton acceptor, free proton donor, and bound proton donor OH stretches, respectively. Calculations by Chaban and Gerber done at CC-VSCF level<sup>22</sup> predict a somewhat different order of intensities:  $|02\rangle_a^+$ ,  $|1\rangle_f|1\rangle_b$ ,  $|2\rangle_f|0\rangle_b$ ,  $|02\rangle_a^+$ , but both studies agree that these four transitions should dominate the  $v_{\text{OH}}=2$  spectrum of  $(\text{H}_2\text{O})_2$ . The strongest  $v_{\text{OH}}=2$  bands in the cyclic water trimer spectrum are predicted to be of the type  $|2\rangle_f|0\rangle_b$  by calculation of Ref. 24. Chaban and Gerber predict that transitions of  $|1\rangle_f|1\rangle_b$  and  $|0\rangle_f|2\rangle_b$  types should be just as strong. Figure 5 shows simulated low-resolution spectra of  $(\text{H}_2\text{O})_2$

TABLE II. Currently accepted gas-phase positions of  $(\text{H}_2\text{O})_2$  stretching fundamentals. The positions are taken from Ref. 10 with  $|01\rangle_a^+$  reassigned to  $|0\rangle_f|1\rangle_b$  based on the results of Ref. 21. The  $|01\rangle_a^+$  transition has only been observed in Ar matrices (Ref. 26), where it is quite weak. Calculations suggest that it should occur at around  $3650\text{ cm}^{-1}$  in gas phase.

Mode	$K' \leftarrow K''$	Position ( $\text{cm}^{-1}$ )
$ 01\rangle_a^-$	$0_{\text{lower}} \leftarrow 1_{\text{lower}}$	3738.4
	$1_{\text{upper}} \leftarrow 0_{\text{upper}}$ and $1_{\text{lower}} \leftarrow 0_{\text{lower}}$	3753
	$2_{\text{upper}} \leftarrow 1_{\text{lower}}$	3777
$ 1\rangle_f 0\rangle_b$	$0_{\text{upper}} \leftarrow 1_{\text{lower}}$ and $1_{\text{lower}} \leftarrow 0_{\text{upper}}$	3731.7
$ 01\rangle_a^+$	Not observed	3633 <sup>a</sup>
$ 0\rangle_f 1\rangle_b$	$0_{\text{upper}} \leftarrow 1_{\text{lower}}$ and $1_{\text{lower}} \leftarrow 0_{\text{upper}}$	3601

<sup>a</sup>Ar matrix.

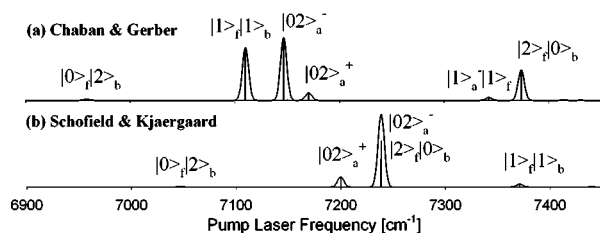


FIG. 5. Predicted band positions and intensities of  $\nu_{\text{OH}}=2$  bands of  $(\text{H}_2\text{O})_2$ . (a) CC-VSCF calculation by Chaban and Gerber (Ref. 22). (b) HCAO calculation by Schofield and Kjaergaard (Ref. 25). For better representation of integrated band intensities, the transitions are convoluted over a Gaussian with half-width at half-maximum (HWHM) =  $7 \text{ cm}^{-1}$ .

based on the prediction of Refs. 22, 24, and 25. Despite a promising concurrence in general theoretical predictions for the overtone intensities, these studies fail to agree on the more detailed relative frequency ordering of the  $(\text{H}_2\text{O})_2$  bands, making spectroscopic assignment of the observed  $(\text{H}_2\text{O})_n$  overtones quite difficult. The most significant disagreement appears to exist for the relative frequencies of the  $|1\rangle_f|1\rangle_b$  and  $|2\rangle_f|0\rangle_b$  overtone bands in both the dimer and trimer species.

The analysis of the  $(\text{H}_2\text{O})_n$  band centered at  $7193 \text{ cm}^{-1}$  may help shed some light on this issue. At higher sensitivity and lower IR pump powers to avoid saturation, this band clearly reveals a partially resolved rotational structure (see Fig. 6), with a characteristic spacing between adjacent lines of roughly  $\approx 0.4 \text{ cm}^{-1}$ . Though not fully resolved, this is nevertheless consistent with an  $a$ -type band for  $(\text{H}_2\text{O})_2$ , which is known to have a near-prolate symmetric top structure with  $B \approx 0.2 \text{ cm}^{-1}$ ,<sup>2,10,13,16</sup> and is clearly inconsistent with any cluster larger than dimer. Simulations of this band profile using the fundamental spectroscopic constants for  $(\text{H}_2\text{O})_2$  quickly reveals it to be composed of at least two overlapping  $a$ -type transitions. Most relevantly to the above discussion, the profile cannot be satisfactorily modeled with overlapping  $b$ - or  $c$ -type transitions, since such bands would be dominated by prominent  $Q$ -branch features not observed in the experimental spectrum.

This lack of strong  $Q$ -branch transitions rules out assignment to the overtone vibration of the hydrogen bond accep-

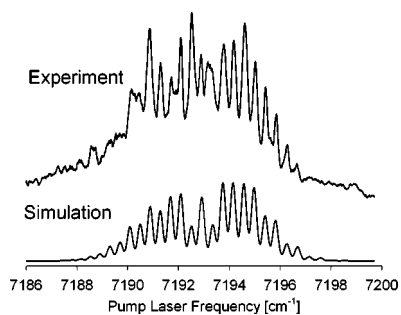


FIG. 6. A slow scan over the  $(\text{H}_2\text{O})_2$  band at  $7193 \text{ cm}^{-1}$ . This band has a partially resolved rotational structure characteristic of a parallel transition in  $(\text{H}_2\text{O})_2$  complex. The band is simulated as a superposition of three  $K=0 \leftarrow 0$  subbands with origins at  $7192.5 \text{ cm}^{-1}$  ( $B_2^-$  subband; odd  $J$ : even  $J=3:6$ ),  $7191.3 \text{ cm}^{-1}$  ( $E$  subband; no alternation),  $7193.3 \text{ cm}^{-1}$  ( $A_2^-$  subband; odd  $J$ : even  $J=6:3$ ) with a linewidth of  $0.25 \text{ cm}^{-1}$ . The band origins are not uniquely determined by the simulation, though a  $B \approx 0.2 \text{ cm}^{-1}$  rotational constant for water dimer is clearly consistent with the observed structure.

tor,  $|02\rangle_a^-$ , since this transition moment would be predominantly along the  $b$  axis of  $(\text{H}_2\text{O})_2$ . In support of this, Huang and Miller<sup>10</sup> only observe  $b$ -type transitions for the corresponding  $|01\rangle_a^-$  fundamental in  $\text{H}_2\text{O}$  dimer (see Table II). Indeed,  $\text{H}_2\text{O}$  dimer exhibits considerable perpendicular structure in the  $|01\rangle_a^-$  fundamental region due to (i)  $K=0_{\text{lower}} \leftarrow 1_{\text{lower}}$ , (ii)  $K=1_{\text{upper}} \leftarrow 0_{\text{upper}}/K=1_{\text{lower}} \leftarrow 0_{\text{lower}}$ , and (iii)  $K=2_{\text{upper}} \leftarrow 1_{\text{lower}}$  subbands, which are observed  $-18 \text{ cm}^{-1}$ ,  $-3 \text{ cm}^{-1}$ , and  $-22 \text{ cm}^{-1}$  away from the  $|01\rangle_a^-$  band origin, respectively. By way of contrast, we do not observe additional  $(\text{H}_2\text{O})_2$  features in this spectral region out to at least  $\pm 40 \text{ cm}^{-1}$  away from the  $7193 \text{ cm}^{-1}$  band. In summary, both the  $7193 \text{ cm}^{-1}$  band shape as well as lack of  $(\text{H}_2\text{O})_2$  transitions in the vicinity make assignment to  $|02\rangle_a^-$  unlikely.

In light of the  $a$ -type rotational contour, a more plausible assignment for the  $7193 \text{ cm}^{-1}$  band is the  $|1\rangle_f|1\rangle_b$  vibration centered on the proton donor unit of  $(\text{H}_2\text{O})_2$ . This vibrational motion promotes a dipole transition moment along the  $a$  axis of  $(\text{H}_2\text{O})_2$ , which is more consistent with the observed band profile. In addition, there is a strong similarity between the band observed here and the  $a$ -type transition profile from Huang and Miller,<sup>10</sup> which has been assigned to  $|0\rangle_f|1\rangle_b$ ,<sup>21</sup> i.e., one quantum of the bound OH stretch. Furthermore, the  $|1\rangle_f|1\rangle_b$  vibration is predicted to be the second strongest OH-stretching overtone in  $(\text{H}_2\text{O})_2$  by Chaban and Gerber<sup>22</sup> and executes a motion that correlates with the strong  $|02\rangle_a^-$  overtone in  $\text{H}_2\text{O}$  monomer. Also, the  $|1\rangle_f|1\rangle_b$  vibrational prediction of  $7110 \text{ cm}^{-1}$  by Chaban and Gerber (see Fig. 5) is in relatively good agreement with experiment. We note that the  $|02\rangle_a^+$  acceptor overtone is yet another possibility for achieving such a strong  $a$ -type transition moment, with predicted band origins [ $7170 \text{ cm}^{-1}$  (Ref. 22) and  $7200 \text{ cm}^{-1}$  (Ref. 25)] in even closer agreement with experiment; however, the predicted overtone intensities are relatively weak in both sets of theoretical calculations.<sup>22,25</sup> In this regard, however, it is worth remembering the “action” nature of these spectra, intensities of which rely on vibrationally mediated UV photolysis of the resulting predissociated complex. For example, excitation of the symmetric  $|02\rangle_a^+$  could well predissociate preferentially into  $\text{H}_2\text{O}$  in  $\nu_{\text{OH}}=1$ , which, in turn, photodissociates efficiently at  $193 \text{ nm}$  to yield OH. We will return to this point later in the discussion but stress the importance of vibrational overtone dynamics in interpreting the spectra. Clearly a predictive understanding of overtone frequencies, intensities, and dynamics in hydrogen-bonded systems remains a challenging area for future progress, which the present work hopes to further stimulate.

With a suggested assignment of the  $7193 \text{ cm}^{-1}$  band structure to either  $|1\rangle_f|1\rangle_b$  or  $|02\rangle_a^+$ , we next address whether one can reproduce the observed rotational profile with known spectroscopic constants of  $(\text{H}_2\text{O})_2$ . Any  $a$ -type transition in  $(\text{H}_2\text{O})_2$  can, in principle, exhibit complicated fine structure because of the presence of five uncoolable nuclear spin symmetry species, specifically three  $K=1 \leftarrow 1_{\text{lower}}$  subbands ( $A_2^-, E^-, B_2^-$ ); three  $K=0 \leftarrow 0_{\text{upper}}$  subbands ( $A_2^-, E^-, B_2^-$ ); and three  $K=0 \leftarrow 0_{\text{lower}}$  subbands ( $A_1^+, E^+, B_1^+$ ). (Note that the specified subband symmetries do not include rotational symmetries unlike the labels shown in Fig. 2.) For example, all of these  $a$ -type subbands appear in close proximity to each

other in far-infrared spectra of acceptor-wag vibration in  $(\text{H}_2\text{O})_2$  and  $(\text{D}_2\text{O})_2$ .<sup>13,49</sup> In practice, the  $A_1^+$  and  $B_1^+$  subbands from  $K=0_{\text{lower}}$  are weak because of low statistical weights (Fig. 2). The  $E$  subbands from  $K=1_{\text{lower}}$  and  $K=0_{\text{upper}}$  are also weak because these levels can relax all the way down to  $K=0_{\text{lower}}$  under supersonic jet conditions. Finally, based on  $\nu_{\text{OH}}=1$  fundamental transitions in  $(\text{H}_2\text{O})_2$ ,<sup>10</sup> the  $K=1 \leftarrow 1$  bands are likely to be significantly broadened by predissociation. Therefore, the dominant  $a$ -type contributions to the rotational structure should come from (i)  $K=0 \leftarrow 0_{\text{upper}} A_2^-$  and  $B_2^-$  and (ii)  $K=0 \leftarrow 0_{\text{lower}} E^+$  subbands.

The  $K=0_{\text{upper}}$  states in the vibrationless  $(\text{H}_2\text{O})_2$  are well understood: the donor-acceptor interchange splitting between  $K=0_{\text{upper}} A_2^-$  and  $B_2^-$  states is  $\approx 0.65 \text{ cm}^{-1}$ .<sup>13,16,50</sup> Although this splitting is known to increase for some intermolecular modes of  $(\text{H}_2\text{O})_2$  that encourage the donor-acceptor interchange,<sup>13</sup> excitation of the OH-stretching states is expected to reduce it significantly. For example, the interchange  $A_2^-/B_2^-$  splitting is just  $0.061 \text{ cm}^{-1}$  in the  $|01\rangle_a^-$   $K=0_{\text{lower}}$  state.<sup>10</sup> Since  $(\text{H}_2\text{O})_2$  retains its plane of symmetry in both  $|1\rangle_f|1\rangle_b$  and  $|02\rangle_a^+$  states, the origin difference of the  $K=0 \leftarrow 0_{\text{upper}} A_2^-$  and  $B_2^-$  subbands should equal the *sum* of the  $K=0 A_2^-/B_2^-$  interchange splittings between lower and upper vibrational states, i.e., on the order of  $0.7\text{--}0.8 \text{ cm}^{-1}$ . Indeed, at our modest resolution,  $a \approx 0.8 \text{ cm}^{-1}$  separation of the  $A_2^-$  and  $B_2^-$  subband origins would nicely, albeit fortuitously, explain the lack of intensity alternation in the spectrum (especially evident in the  $R$ -branch region), because of cancellation at low  $J$  of the predicted  $B_2^- J_{\text{even}}/J_{\text{odd}}=6/3$  vs  $A_2^- J_{\text{even}}/J_{\text{odd}}=3/6$  nuclear spin statistical ratios.

In the interest of simplicity, therefore, we have modeled the observed transition profile as a combination of (i) two  $K=0 \leftarrow 0_{\text{upper}} A_2^-$  and  $B_2^-$  subbands, separated by  $\approx 0.8 \text{ cm}^{-1}$  and (ii) one  $K=0 \leftarrow 0_{\text{lower}} E^+$  subband, with the relative location of the  $K=0 \leftarrow 0_{\text{lower}}$  and  $K=0 \leftarrow 0_{\text{upper}}$  subbands treated as an adjustable parameter. Each  $(\text{H}_2\text{O})_2$  subband is calculated as a near prolate symmetric top with rotational parameters taken from Ref. 10, with the result shown in Fig. 6. The simulation is consistent with a  $7 \pm 3 \text{ K}$  rotational temperature (same as for Ar- $\text{H}_2\text{O}$  bands discussed below) and readily reproduces several salient features of the observed band, namely, (i) parallel structure, (ii) absence of a band gap, and (iii) no obvious intensity alternation. However, with the present instrumental resolution, the simulation is not very sensitive to the transition band origins, which thus remain poorly determined. Nevertheless, the rotational structure clearly confirms the carrier of the observed band to be  $(\text{H}_2\text{O})_2$  that we can tentatively assign to either the  $|1\rangle_f|1\rangle_b$  or  $|02\rangle_a^+$  overtone vibration.

Inspection of the spectrum in Fig. 4 indicates the potential presence of several other  $(\text{H}_2\text{O})_n$  bands, the assignment of which requires identification or suppression of the much stronger Ar- $\text{H}_2\text{O}$  transitions. Since the water complexes predissociate much faster than the laser pulse duration (see below), the Ar- $\text{H}_2\text{O}$  bands can be largely suppressed by recording the spectrum using very small IR pump-UV photolysis delays. This procedure reveals that the bands at  $7240$ ,  $7250$ , and  $7282 \text{ cm}^{-1}$  can be ascribed to  $(\text{H}_2\text{O})_n$  complexes that, based on both theoretical predictions and matrix

studies, most likely correspond to  $|2\rangle_f|0\rangle_b$  transitions in water dimer (Table I). Specifically, Perchard reported a strong band at  $7236 \text{ cm}^{-1}$  in argon matrix<sup>26</sup> and a corresponding band at  $7220 \text{ cm}^{-1}$  in nitrogen matrix,<sup>27</sup> which he assigned to  $|2\rangle_f|0\rangle_b$  overtone of the proton donor unit as well. His assignments were recently corroborated by HCAO calculations.<sup>25</sup> CC-VSCF calculations of Chaban and Gerber place this band higher in frequency but also predict a large transition strength for  $|2\rangle_f|0\rangle_b$ .<sup>22</sup> The present gas-phase studies provide some additional information; in particular, the  $7240$  and  $7250 \text{ cm}^{-1}$  bands appear perpendicular which is consistent with  $|2\rangle_f|0\rangle_b$  vibrational motion predominantly along the  $c$  axis. The subband spacings and rotational contours are consistent with a  $|2\rangle_f|0\rangle_b$  overtone band assignment, but based on theoretical predictions, it could, in principle, arise from the acceptor  $|02\rangle_a^-$  band. Further theoretical efforts in this overtone region would be extremely useful to settle these issues.

There has been a lot of interest in the spectroscopic quantification of  $(\text{H}_2\text{O})_2$  in the atmosphere via its overtone transitions.<sup>35</sup> In view of the difficulties associated with precise theoretical predictions of  $(\text{H}_2\text{O})_2$  overtone frequencies and intensities, it is challenging to assign features observed in atmospheric transmission spectra to  $(\text{H}_2\text{O})_2$  with certainty.<sup>26</sup> Present observation of a rotationally resolved overtone of  $(\text{H}_2\text{O})_2$  is an important step towards resolving this problem. Although the proximity of the  $|1\rangle_f|1\rangle_b$  band of  $(\text{H}_2\text{O})_2$  to free  $\text{H}_2\text{O}$  transitions reduces its potential usefulness for observational work on  $(\text{H}_2\text{O})_2$  in the atmosphere, it is the only known rotationally resolved overtone transition rigorously assigned to  $(\text{H}_2\text{O})_2$ . High-resolution spectra of  $(\text{H}_2\text{O})_2$  overtones, such as  $\nu_{\text{OH}}=3$ , should be even more useful for the observational studies, and this is where future efforts of spectroscopists studying  $(\text{H}_2\text{O})_2$  should be directed.

#### D. Overtone ( $\nu_{\text{OH}}=2$ ) spectra of Ar- $\text{H}_2\text{O}$

The vibrationally mediated IR spectra in Fig. 4 are clearly dominated by transitions of Ar- $\text{H}_2\text{O}$  van der Waals clusters, to which we now turn our attention. Indeed, a question worth raising is why the spectra of such weakly bound van der Waals complexes can be so *prominent* over the much more strongly bound  $(\text{H}_2\text{O})_n$  species, even though the latter are likely present in much higher concentrations. The answer almost certainly has to do with the vibrationally mediated nature of the action spectroscopy that requires the IR photon to enhance the subsequent  $193 \text{ nm}$  photodissociation of  $\text{H}_2\text{O}$ , either in the complex or its predissociated fragments. This enhancement, in turn, depends very sensitively on the number of quanta in OH stretch excitation in the  $\text{H}_2\text{O}$  subunit, as beautifully elucidated by Crim co-workers.<sup>36,44,51</sup> For an atom-polyatom species such as Ar- $\text{H}_2\text{O}$ , predissociation at the first overtone level occurs on a relatively slow time scale ( $\approx 10\text{--}100 \text{ ns}$ , depending on the specific internal rotor quantum state excited that, with  $7 \text{ ns}$  laser time resolution, readily permits efficient photolysis of  $\text{H}_2\text{O}$  in the  $\nu_{\text{OH}}=2$  manifold). Furthermore,  $\Delta\nu_{\text{OH}}=-1$  predissociation of the weakly bound Ar- $\text{H}_2\text{O}$  complex ( $D_0 \approx 140 \text{ cm}^{-1}$ ) (Ref. 42) most likely

yields H<sub>2</sub>O in a near resonant vibrational state with  $\nu_{\text{OH}}=1$ , and thus still exhibiting the necessary photolysis enhancement. H<sub>2</sub>O dimer, on the other hand, is more strongly bound ( $D_0 \approx 1700 \text{ cm}^{-1}$ ),<sup>18</sup> predissociates rapidly (*vide infra*), and has more channels with which to deposit the excess overtone energy. The net effect is a decreased efficiency for detecting H<sub>2</sub>O dimer by first overtone vibrationally mediated photolysis; this effect explains preferential sensitivity to weakly bound species such as Ar–H<sub>2</sub>O, H<sub>2</sub>–H<sub>2</sub>O, etc. Furthermore, it also rationalizes the absence in our spectra of clusters beyond (H<sub>2</sub>O)<sub>2</sub>, since predissociation is statistically less likely to deposit sufficient OH-stretching internal energy in the H<sub>2</sub>O fragments required for subsequent photofragmentation. Interestingly, this also bodes well for vibrationally mediated action spectroscopy of H<sub>2</sub>O dimer and larger clusters in the *second* region overtone region for which a significant gain in detection sensitivity would be predicted.

High-resolution rovibrational spectroscopy of Ar–H<sub>2</sub>O has been well studied at the ground state ( $\nu_{\text{OH}}=0$ ) and first excited state ( $\nu_{\text{OH}}=1$ ) levels of H<sub>2</sub>O,<sup>11,40,42,47,48,52</sup> revealing a weakly anisotropic potential and states best described by H<sub>2</sub>O quantum numbers in the free rotor limit. Under jet-cooled conditions, one therefore expects to observe only transitions originating from the lowest *para*  $\Sigma(0_{00})$  and *ortho*  $\Sigma(1_{01})$  states of the complex, with weaker transitions also possible from the incompletely cooled *ortho*  $\Pi(1_{01})$  state [which lies  $11.4 \text{ cm}^{-1}$  above  $\Sigma(1_{01})$ ]. Transitions built upon the stronger  $|02\rangle^-$  band of H<sub>2</sub>O monomer should dominate those derived from the weaker  $|02\rangle^+$  and  $|11\rangle^+$  overtone bands. Based on these expectations and on analogy with spectra of Ar–H<sub>2</sub>O in the  $\nu_{\text{OH}}=1$  (Refs. 11 and 47) and  $\nu_{\text{OH}}=3$  spectral ranges,<sup>40</sup> it is relatively straightforward to assign many of the bands to Ar–H<sub>2</sub>O (Table I).

As predicted, the most prominent Ar–H<sub>2</sub>O bands correlate with the  $|02\rangle^- 0_{00} \leftarrow 1_{01}$  and  $|02\rangle^- 1_{01} \leftarrow 0_{00}$  lines of H<sub>2</sub>O monomer, just as seen in previous studies of fundamental  $|01\rangle^-$  (Refs. 11 and 47) and second overtone  $|03\rangle^-$  (Ref. 40) (Fig. 4). Due to weak potential anisotropy contributions from the Ar atom, the threefold spatial degeneracy of the  $1_{01}$  internal rotor state of H<sub>2</sub>O splits into  $\Pi$  and  $\Sigma$  components, yielding  $\Sigma(0_{00}) \leftarrow \Pi(1_{01}) (7218.45 \text{ cm}^{-1})$  and  $\Sigma(0_{00}) \leftarrow \Sigma(1_{01}) (7230.05 \text{ cm}^{-1})$  subbands “flanking” the  $|02\rangle^- 0_{00} \leftarrow 1_{01}$  monomer transition. As this lifting of spatial degeneracy by Ar also occurs in the  $|02\rangle^- 1_{01}$  upper state, one similarly predicts two Ar–H<sub>2</sub>O bands surrounding the  $|02\rangle^- 1_{01} \leftarrow 0_{00}$  monomer line, as is indeed observed at  $7263.7 \text{ cm}^{-1}$  [ $\Sigma(1_{01}) \leftarrow \Sigma(0_{00})$ ] and  $7275.0 \text{ cm}^{-1}$  [ $\Pi(1_{01}) \leftarrow \Sigma(0_{00})$ ]. Further confirmation of these assignments can be obtained from the presence (or absence) of sharp central  $Q$  branches in these bands, respectively, in agreement with the predicted perpendicular and parallel nature of the  $\Sigma \leftarrow \Pi$  and  $\Sigma \leftarrow \Sigma$  transition moments (see Table I).

Similar to what was previously demonstrated for H<sub>2</sub>O dimer, the rotational constants of this van der Waals complex are sufficiently large to permit rotational analysis of favorable bands, providing unambiguous additional confirmation of the species as Ar–H<sub>2</sub>O. For example, a higher resolution scan of the  $\Sigma(0_{00}) \leftarrow \Sigma(1_{01})$  band at  $7230.05 \text{ cm}^{-1}$  is shown in Fig. 7, which can be well modeled using known rotational

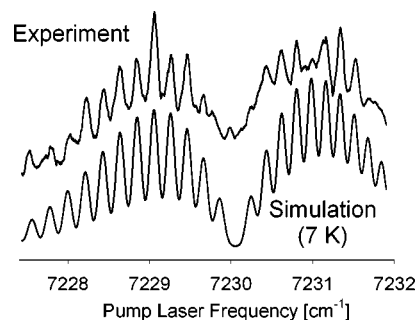


FIG. 7. Sample scan over the Ar–H<sub>2</sub>O  $|02\rangle^- \Sigma(0_{00}) \leftarrow |00\rangle^+ \Sigma(1_{01})$  band. The profile is best described by a rotational temperature of 7 K, with a rotational line numbering certain to  $\pm 1J$ . Simulation linewidth is  $0.15 \text{ cm}^{-1}$ , which is the laser resolution limit.

constants of Ar–H<sub>2</sub>O (Refs. 11 and 48) and a typical rotational temperature of 7 K. From the observed splitting between  $|02\rangle^- \Sigma(0_{00}) \leftarrow \Pi(1_{01})$  and  $|02\rangle^- \Sigma(0_{00}) \leftarrow \Sigma(1_{01})$  bands, we can derive the energy separation of  $11.6 \pm 0.3 \text{ cm}^{-1}$  between  $J=1 \Pi(1_{01})$  and  $J=1 \Sigma(1_{01})$  in  $|00\rangle^+$  state, in good agreement with the value of  $11.333 \text{ cm}^{-1}$  obtained from high-resolution study of Ar–H<sub>2</sub>O fundamentals by Lascola and Nesbitt.<sup>11</sup> From the  $|02\rangle^- \Sigma(1_{01}) \leftarrow \Sigma(0_{00})$  and  $|02\rangle^- \Pi(1_{01}) \leftarrow \Sigma(0_{00})$  band positions, one can also infer the corresponding splitting in the upper  $|02\rangle^-$  state to be  $11.3 \pm 0.3 \text{ cm}^{-1}$ , i.e., consistent with only minor changes in the anisotropy of the Ar–H<sub>2</sub>O intermolecular potential upon OH stretch excitation.

The effect of the H<sub>2</sub>O vibration on the Ar–H<sub>2</sub>O potential well depth is similarly small as evidenced by a redshift of only  $2.9 \pm 0.3 \text{ cm}^{-1}$  between the  $|02\rangle^- \Sigma(0_{00}, J=0) \leftarrow |00\rangle^+ \Sigma(0_{00}, J=0)$  band origins in free H<sub>2</sub>O and in Ar–H<sub>2</sub>O. The sign of the frequency shift is consistent with a slightly stronger van der Waals bond in the  $|02\rangle^-$  state. The magnitude of the frequency shift is intermediate between that for the  $|01\rangle^-$  transition ( $\Delta\nu = 1.32 \text{ cm}^{-1}$ ) (Ref. 11) and  $|03\rangle^-$  transition ( $\Delta\nu = 3.06 \text{ cm}^{-1}$ ) (Ref. 40) indicating a systematic increase in the Ar–H<sub>2</sub>O intermolecular bond strength with  $\nu_{\text{OH}}$ . This behavior is qualitatively consistent with observations on other atom-polyatom van der Waals complexes such as Ar–HF.<sup>53</sup>

The strong set of band(s) near  $7293 \text{ cm}^{-1}$  can also be assigned to Ar–H<sub>2</sub>O that, by proximity to the  $|02\rangle^- 2_{02} \leftarrow 1_{01}$  monomer transition at  $7294.14 \text{ cm}^{-1}$ , probably arises from one or more projection components,  $\Sigma$ ,  $\Pi$ ,  $\Delta$  of the internal H<sub>2</sub>O rotor subunit along the intermolecular axis. Detailed assignment of the much weaker band structures (for example, near  $7234$ ,  $7254$ , and  $7258 \text{ cm}^{-1}$ ) is less certain. However, proximity to the  $|02\rangle^+ 1_{11} \leftarrow 0_{00}$  and  $|02\rangle^+ 2_{12} \leftarrow 1_{01}$  lines of water monomer clearly suggests that they are built on these transitions. What would make this dynamically interesting is that the  $|02\rangle^+$  overtone band in the monomer is extremely weak, i.e., the  $|02\rangle^+ 1_{11} \leftarrow 0_{00}$  and  $|02\rangle^- 1_{01} \leftarrow 0_{00}$  line intensities differ by more than two orders of magnitude, yet the corresponding Ar–H<sub>2</sub>O bands built on  $|02\rangle^+$  and  $|02\rangle^-$  vibrations have much more comparable intensities in action spectrum. In fact, this effect appears to be so strong for  $|02\rangle^+ 1_{11} \leftarrow 0_{00}$  that we see in Fig. 4 vibrationally mediated photodissociation of the Ar–H<sub>2</sub>O cluster but not of bare

H<sub>2</sub>O monomer. One can attribute this unusual intensity pattern to the difference in predissociation dynamics of Ar–H<sub>2</sub>O from  $|02\rangle^+$  and  $|02\rangle^-$  states. Indeed, if the action spectrum is recorded using  ${}^2\Pi_{3/2}^-(N=2)$  rotational state of OH instead of  $N=8$ , the intensity of Ar–H<sub>2</sub>O  $|02\rangle^+$  bands relative to that of  $|02\rangle^-$  bands is substantially reduced, suggesting that predissociation of Ar–H<sub>2</sub>O  $|02\rangle^+$  states produces more rotational and bending excitation in the water monomer.<sup>43</sup> Experimental efforts to further elucidate these weaker band assignments are currently being pursued, based on product state distributions and predissociation lifetimes and will be presented elsewhere.<sup>54</sup>

### E. Vibrational predissociation dynamics

Vibrationally mediated spectroscopy also permits one to *directly* measure predissociation lifetimes of complexes by monitoring the final photofragment (OH) as a function of the time delay between the near-infrared pump and UV photolysis lasers. The UV photodissociation of H<sub>2</sub>O takes place on a femtosecond time scale, so the rise time for OH formation following the UV pulse can be completely neglected on the nanosecond time scale of our experiment. For typical laser pulse durations, molecular jet velocities of  $\approx 10^5$  cm/s, and laser beam sizes of 1–3 mm, this technique can therefore straightforwardly access the time window between  $\Delta t \approx 7$  and 1000 ns. The lower limit is determined by the finite pulse duration (5–7 ns), whereas the upper limit corresponds to the “flyout” time for excited molecules to exit the probe volume. The Ar–H<sub>2</sub>O overtone states observed here conveniently result in predissociation within this time window.

By way of illustration, we consider the  $|02\rangle^- \Sigma(0_{00}) \leftarrow \Sigma(1_{01})$  transition in Ar–H<sub>2</sub>O (see Fig. 8). If the initially prepared Ar–H<sub>2</sub>O complex  $|02\rangle^- \Sigma(0_{00})$  photodissociates into *different* OH states than photolysis of the predissociated H<sub>2</sub>O monomer distribution, the OH distributions will depend on the pump-photolysis delay. If photolysis occurs before predissociation, the OH distribution reflects the break up of the Ar–H<sub>2</sub>O cluster. At the other extreme, if photolysis occurs long after predissociation, the OH distributions reflect dynamics of the H<sub>2</sub>O( $v'$ ) predissociation product. Signals probed on a single quantum state of OH reflect the superposition of both intracluster and predissociated cluster photolysis dynamics as function of time delay. Since Ar–H<sub>2</sub>O predissociation tends to produce bend-excited H<sub>2</sub>O (see below), which then photofragments to form rotationally hotter OH distributions, one expects OH LIF signal to *increase* for high  $N$  and *decrease* for low  $N$  with pump-photolysis delay.

These trends are nicely verified in Fig. 8, which shows OH  ${}^2\Pi_{3/2}^-(N=8)$  and  ${}^2\Pi_{3/2}^-(N=2)$  populations after the  $|02\rangle^- \Sigma(0_{00}) \leftarrow \Sigma(1_{01})$  overtone excitation of Ar–H<sub>2</sub>O. The  $N=2$  signal rises quickly at  $t=0$ , as this state is produced in direct vibrationally mediated dissociation of Ar–H<sub>2</sub>O, but then decays to a constant level characteristic of the photolysis of the H<sub>2</sub>O predissociation product. The  $N=8$  signal starts out at zero because direct dissociation of Ar–H<sub>2</sub>O in  $|02\rangle^- \Sigma(0_{00})$  state does not produce such hot OH states, but it then rises to a steady level also determined by the H<sub>2</sub>O predissociation product. Both sets of data can be least squares fit

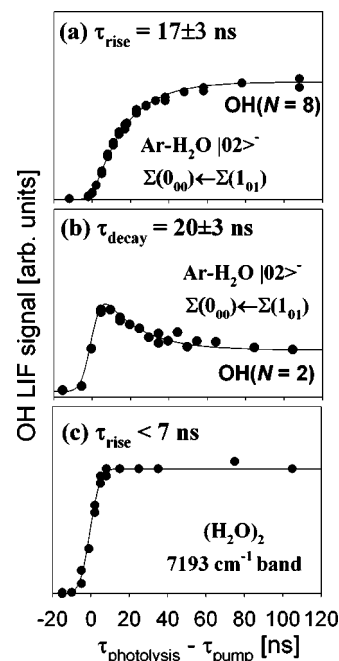


FIG. 8. Predissociation lifetimes of Ar–H<sub>2</sub>O and (H<sub>2</sub>O)<sub>2</sub>. The observed OH ( $N$ ) signal comes from two independent channels: vibrationally mediated photodissociation and predissociation followed by photodissociation (see Fig. 1). (a) Only predissociation/photodissociation channel contributes to the rise of high- $N$  states of OH in the Ar–H<sub>2</sub>O case. (b) Vibrationally mediated photodissociation is responsible for the rapid rise and the predissociation/photodissociation for the slower decay of the signal for low- $N$  states of OH in the Ar–H<sub>2</sub>O case. (c) Rapid predissociation of (H<sub>2</sub>O)<sub>2</sub> followed by direct photolysis of the vibrationally excited H<sub>2</sub>O predissociation fragments results in appearance of OH on a time scale of  $< 7$  ns.

to an exponential rise or decay, clearly demonstrating that the complexes undergo predissociation on a  $18 \pm 5$  ns time scale. Note that this is essentially identical to the  $16 \pm 5$  ns predissociation lifetime for  $|03\rangle^- \Sigma(0_{00})$  states<sup>55</sup> observed in a similar real time measurement. Also relevant in this regard are high-resolution measurements on the  $|01\rangle^- \Sigma(0_{00})$  state of Ar–H<sub>2</sub>O from which a lower limit of 16 ns is extracted from linewidth studies.<sup>11</sup> At first this seems dynamically surprising; from Fermi’s golden rule, one might anticipate rapidly increasing predissociation rates with increasing internal energy. However, the vibrational density of states at these energies is still extremely sparse, and thus the predissociation dynamics in Ar–H<sub>2</sub>O are likely to be highly nonstatistical, resulting in long lifetimes sensitive to local resonances between the initial cluster and final H<sub>2</sub>O distributions. In support of this picture, a more complete study currently underway (Ref. 43) of the other Ar–H<sub>2</sub>O bands in the  $v_{\text{OH}}=2$  region exhibit lifetimes that vary more or less erratically with vibration and internal rotor quantum state.

By way of comparison, Fig. 8(c) shows the corresponding time-delay dependence for the 7193 cm<sup>-1</sup> band of (H<sub>2</sub>O)<sub>2</sub>. In contrast to Ar–H<sub>2</sub>O, the  $v_{\text{OH}}=2$  excitation of (H<sub>2</sub>O)<sub>2</sub> results in an instrumentally limited appearance of OH for all  $N$ . Indeed, this dynamical difference was exploited in the preceding section to selectively discriminate in the action spectra between long lived Ar–H<sub>2</sub>O excitations from shorter lived (H<sub>2</sub>O)<sub>2</sub> ones and is consistent with a rapid predissociation of the complex on a time scale  $< 7$  ns. The

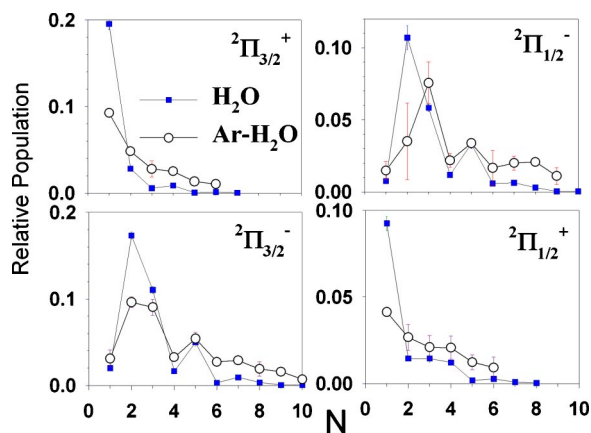


FIG. 9. Quantum-state distribution of all spin-orbit, lambda-doublet, and rotational OH states resulting from vibrationally mediated dissociation of Ar–H<sub>2</sub>O following excitation in the  $|02\rangle^- \Sigma(0_{00}) \leftarrow \Sigma(1_{01})$  band (filled squares). Compared to the results for  $|02\rangle^- 0_{00} \leftarrow 1_{01}$  excitation in free H<sub>2</sub>O (open circles), dissociation inside the complex produces slightly hotter and more statistical OH.

observations could also be explained by postulating a very long ( $>1 \mu\text{s}$ ) predissociation lifetime, but this scenario is highly unlikely in view of the rapid predissociation rates of (H<sub>2</sub>O)<sub>2</sub> in the  $\nu_{\text{OH}}=1$  manifold.<sup>10</sup>

For pump-photolysis time delays much shorter than the predissociation lifetime, these vibrationally mediated photolysis methods permit one to investigate intramolecular collision dynamics in a single size-selected and quantum-state-selected cluster. For example, dissociation of free H<sub>2</sub>O in  $|02\rangle^-$  states is known to result in rotationally cold OH (see Fig. 9) with the distribution peaked at  $N=1-3$ .<sup>43</sup> Indeed, the action spectrum (Fig. 4) would be dominated by free H<sub>2</sub>O lines if a rotationally cold state of OH (e.g.,  $N=2$ ) was used in the probing step instead of  $N=8$ . With vibrationally mediated photolysis, one can measure the distribution of OH produced via dissociation of Ar–H<sub>2</sub>O complexes via the  $|02\rangle^- \Sigma(0_{00}) \leftarrow \Sigma(1_{01})$  transition and directly compare with photolysis of the “bare” internal rotor  $|02\rangle^- \Sigma(0_{00})$  excited H<sub>2</sub>O monomer in the *absence* of the Ar atom. This data is summarized in Fig. 9 for each of the spin-orbit and lambda-doublet states and reveals two interesting features. First of all, there are considerably higher populations in each electronic sublevel at high  $N$ , consistent with intracuster *rotational* excitation of the recoiling OH prior to exiting the cluster. Second, the strong oscillations in  $N$  for the various electronic sublevels (most apparent in the  $2\Pi_{3/2/1/2}^-$  manifolds) have much lower contrast ratios for the cluster vs free monomer photodissociation processes. This implies less specificity in branching ratio into a given electronic manifold that is consistent with partial scrambling of the nascent electronic state distributions, but this time reflecting *nonadiabatic* collisional dynamics inside the cluster. These results confirm those obtained on Ar–H<sub>2</sub>O clusters in the second overtone region<sup>40</sup> and which has been nicely modeled by inelastic (rotational and electronic state changing) collisions between the recoiling OH and Ar atom within the complex.<sup>40,41</sup>

For pump-photolysis delays (200–500 ns) much longer than the vibrational predissociation lifetime ( $18 \pm 5$  ns), a

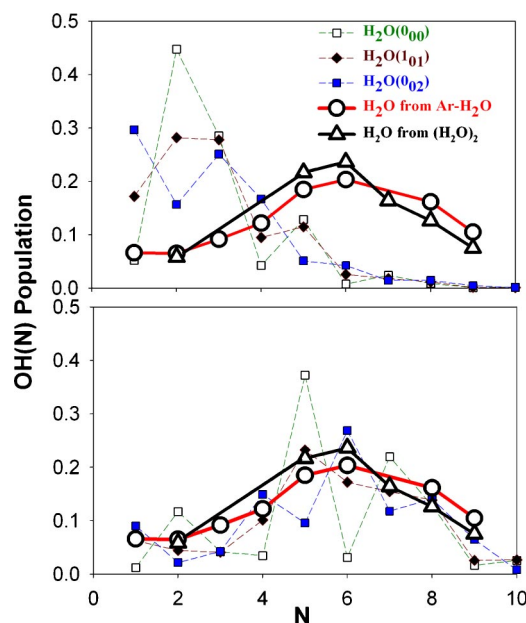
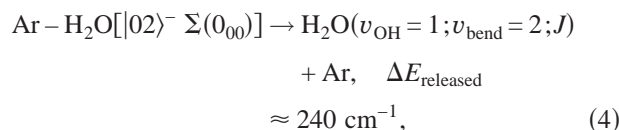


FIG. 10. Rotational distribution of  $2\Pi_{3/2}^-(N)$  states of OH resulting from UV photolysis of H<sub>2</sub>O( $\nu'$ ) produced in predissociation of Ar–H<sub>2</sub>O [ $|02\rangle^- \Sigma(0_{00})$  state; large circles] and (H<sub>2</sub>O)<sub>2</sub> (7193 cm<sup>-1</sup> band; large triangles). Also shown are the corresponding OH state distributions resulting from direct photolysis of individual quantum states of free H<sub>2</sub>O ( $J=0, 1, 2$ ) in  $|02\rangle^-$  state (top panel) and  $|01^-(2)\rangle$  state (bottom panel) (Ref. 43). Explicit comparison suggests that H<sub>2</sub>O( $\nu_{\text{OH}}=0, 1; \nu_{\text{bend}}=2$ ) is the dominant product of predissociation of Ar–H<sub>2</sub>O and (H<sub>2</sub>O)<sub>2</sub>.

completely different picture of the OH quantum state distributions emerges (see Fig. 10). By this time, all initially excited Ar–H<sub>2</sub>O complexes [ $|02\rangle^- \Sigma(0_{00})$ ] have predissociated, and the OH products are generated by UV photolysis from nascent H<sub>2</sub>O( $\nu'$ ) molecules. As clearly evident in Fig. 10 (shown for the  $2\Pi_{3/2}^-$  manifold), the OH distribution is now dramatically hotter, peaking at around  $N=6$ . Interestingly, a qualitatively similar distribution is also seen for vibrationally mediated photolysis on the H<sub>2</sub>O dimer bands, again showing a strong preference for highly rotationally excited OH and suggesting a qualitatively similar predissociation pathway. Although our experiment does not probe these H<sub>2</sub>O( $\nu'$ ) distribution directly, we can nevertheless glean some insight into the nature of the states formed from the predissociation event by comparison with systematic vibrationally mediated photolysis studies of H<sub>2</sub>O rotational and vibrational quantum states. Specifically, Fig. 10(a) displays 193 nm photolysis OH product state distributions ( $2\Pi_{3/2}^-$ ) from  $J_{K_a K_c}=0_{00}, 1_{01}$ , and  $2_{02}$  rotational states of H<sub>2</sub>O, each excited to the  $|02\rangle^-$  overtone level. Consistent with similar results by Crim and co-workers for  $|04\rangle^-$  excited H<sub>2</sub>O,<sup>51</sup> these results indicate a slight, but systematic, warming of the OH distributions with initial H<sub>2</sub>O rotation. However, the shape of these distributions is qualitatively much colder than observed experimentally.

In marked contrast, Fig. 10(b) exhibits OH distributions from vibrationally mediated photolysis of H<sub>2</sub>O for the same series of rotational levels, but now in  $|01^-(2)\rangle$ , i.e., a nearly isoenergetic combination state corresponding to (i) OH stretch fundamental plus (ii) two quanta of HOH bending excitation. These OH distributions are now substantially hot-

ter, peaking at  $N \approx 5-6$ , and qualitatively much more consistent with the Ar–H<sub>2</sub>O dimer results. Although further experiments will be necessary to establish this definitively, the results plausibly suggest that vibrational predissociation of Ar–H<sub>2</sub>O from  $|02\rangle^- \Sigma(0_{00})$  has strong contributions from the near resonant V–V pathway:



which would then photofragment into the high- $N$  OH distributions observed in Fig. 10. The smoothness of the resulting OH state distribution would also be consistent with several different  $J$  states produced in Eq. (4), since photolysis of single  $J$  states of H<sub>2</sub>O generally result in much more structured OH quantum state distributions (for example, see Figs. 9 and 10). As a final comment, it is worth noting that the OH state distributions resulting from the photolysis of overtone excited (H<sub>2</sub>O)<sub>2</sub> (i.e., 7193 cm<sup>-1</sup> band) are remarkably similar to the above results for Ar–H<sub>2</sub>O. This might again suggest substantial bending excitation in one or more of the HOH products. Because of the higher binding energy of (H<sub>2</sub>O)<sub>2</sub> vs Ar–H<sub>2</sub>O ( $D_0 \approx 1700 \text{ cm}^{-1}$  vs  $140 \text{ cm}^{-1}$ ), however, predissociation into same H<sub>2</sub>O( $v_{\text{OH}}=1; v_{\text{bend}}=2; J$ ) states is now not energetically possible. Nevertheless, several bend-excited channels remain energetically open such as formation of H<sub>2</sub>O( $v_{\text{OH}}=0; v_{\text{bend}} \leq 3$ ) and H<sub>2</sub>O( $v_{\text{OH}}=1; v_{\text{bend}} \leq 1$ ). Based on the requirement of vibrationally enhanced photodissociation cross section at 193 nm, the observed distributions plausibly arise from photolysis of H<sub>2</sub>O( $v_{\text{OH}}=1; v_{\text{bend}} \leq 1, J$ ). However, it is worth noting that since the action spectra derive both their sensitivity and specificity from strong vibrationally mediated skewing of the photodissociation cross sections, this need not be representative of the full distribution of predissociated H<sub>2</sub>O. Nevertheless, these studies make simple predictions and highlight some interesting directions for further exploration with quantum state resolution in the ejected H<sub>2</sub>O, as perhaps could be studied by IR photofragmentation recoil spectroscopy.<sup>56,57</sup>

#### IV. CONCLUSION AND SUMMARY

The combination of slit jet expansions with (i) IR pump vibrational excitation, (ii) vibrationally selective excimer photolysis, followed by (iii) state-resolved laser-induced fluorescence probing of fragments, reveals itself as a powerful spectroscopic tool for extending traditional vibrationally mediated photodissociation methods into the overtone region of the water clusters. Rich vibrational structure has been observed in vibrationally mediated dissociation spectra of H<sub>2</sub>O/Ar mixtures under supersonically cooled conditions in the vicinity of the first OH-stretching overtones of H<sub>2</sub>O. The observed resonances can be assigned to overtone transitions of Ar–H<sub>2</sub>O and (H<sub>2</sub>O)<sub>2</sub> based on their spectral structure and photodissociation dynamics and, in favorable cases, even permitting direct detection of resolved rotational structure. Indeed, this is the first reported gas-phase spectra of H<sub>2</sub>O

dimer overtone in the gas phase that reveals both agreement and disagreement with currently available theoretical models.

The use of time delayed IR pump and photolysis lasers allows direct observation of predissociation dynamics of H<sub>2</sub>O complexes on the 10 ns  $1 \mu\text{s}$  time scale, as demonstrated on  $v_{\text{OH}}=2$  of Ar–H<sub>2</sub>O clusters. For sufficiently long lived vibrational states, this method provides a novel scheme for initiating photochemical events inside size-selected and quantum-state-selected clusters. In conjunction with parallel studies of the isolated monomer, solvent effects on the photofragmentation dynamics of H<sub>2</sub>O can be directly probed by comparison with vibrationally mediated photodissociation of the same free rotor state H<sub>2</sub>O state in the absence of the perturbing Ar atom. Specifically, vibrationally mediated dissociation of H<sub>2</sub>O within Ar–H<sub>2</sub>O complex clearly produces *hotter* rotational OH distributions as well as promoting partial *nonadiabatic* energy transfer between  $\Pi_{3/2,1/2}$  and lambda-doublet electronic levels. A simple physical model for this would be intracuster collisions between the recoiling OH photofragment and Ar atom.<sup>40,41</sup> At a more challenging level, however, these data reflect the detailed photofragmentation dynamics of H<sub>2</sub>O in the presence of a single solvent atom, yet with the considerable spectroscopic simplification of aligned, fully quantum-state-selected reagents as well as the special intracuster advantage of well-determined impact parameter and total angular momentum.

#### ACKNOWLEDGMENTS

Financial support by the National Science Foundation and Air Force Office of Scientific Research is gratefully acknowledged. A.E.W.K. wishes to acknowledge gratitude to JILA for Visiting Fellowship support during the time of this research.

<sup>1</sup>M. Van Thiel, E. D. Becker, and G. C. Pimentel, J. Chem. Phys. **27**, 486 (1957).

<sup>2</sup>T. R. Dyke and J. S. Muentzer, J. Chem. Phys. **60**, 2929 (1974).

<sup>3</sup>T. R. Dyke, K. M. Mack, and J. S. Muentzer, J. Chem. Phys. **66**, 498 (1977).

<sup>4</sup>T. R. Dyke, J. Chem. Phys. **66**, 492 (1977).

<sup>5</sup>R. H. Page, J. G. Frey, Y. R. Shen, and Y. T. Lee, Chem. Phys. Lett. **106**, 373 (1984).

<sup>6</sup>M. F. Vernon, D. J. Krajnovich, H. S. Kwok, J. M. Lisy, Y. R. Shen, and Y. T. Lee, J. Chem. Phys. **77**, 47 (1982).

<sup>7</sup>D. F. Coker, R. E. Miller, and R. O. Watts, J. Chem. Phys. **82**, 3554 (1985).

<sup>8</sup>S. Wuelfert, D. Herren, and S. Leutwyler, J. Chem. Phys. **86**, 3751 (1987).

<sup>9</sup>Z. S. Huang and R. E. Miller, J. Chem. Phys. **88**, 8008 (1988).

<sup>10</sup>Z. S. Huang and R. E. Miller, J. Chem. Phys. **91**, 6613 (1989).

<sup>11</sup>R. Lascola and D. J. Nesbitt, J. Chem. Phys. **95**, 7917 (1991).

<sup>12</sup>J. B. Paul, R. A. Provencal, and R. J. Saykally, J. Phys. Chem. A **102**, 3279 (1998).

<sup>13</sup>L. B. Braly, K. Liu, M. G. Brown, F. N. Keutsch, R. S. Fellers, and R. J. Saykally, J. Chem. Phys. **112**, 10314 (2000).

<sup>14</sup>K. L. Busarow, R. C. Cohen, G. A. Blake, K. B. Laughlin, Y. T. Lee, and R. J. Saykally, J. Chem. Phys. **90**, 3937 (1989).

<sup>15</sup>R. C. Cohen and R. J. Saykally, J. Phys. Chem. **96**, 1024 (1992).

<sup>16</sup>L. H. Coudert and J. T. Hougen, J. Mol. Spectrosc. **139**, 259 (1990).

<sup>17</sup>G. T. Fraser, R. D. Suenram, and L. H. Coudert, J. Chem. Phys. **90**, 6077 (1989).

<sup>18</sup>R. S. Fellers, C. Leforestier, L. B. Braly, M. G. Brown, and R. J. Saykally, Science **284**, 945 (1999).

- <sup>19</sup>N. Goldman, R. S. Fellers, C. Leforestier, and R. J. Saykally, *J. Phys. Chem. A* **105**, 515 (2001).
- <sup>20</sup>G. C. Groenenboom, E. M. Mas, R. Bukowski, K. Szalewicz, P. E. S. Wormer, and A. van der Avoird, *Phys. Rev. Lett.* **84**, 4072 (2000).
- <sup>21</sup>F. Huisken, M. Kaloudis, and A. Kulcke, *J. Chem. Phys.* **104**, 17 (1996).
- <sup>22</sup>G. Chaban and R. Gerber (private communication).
- <sup>23</sup>H. C. W. Tso, D. J. W. Geldart, and P. Chylek, *J. Chem. Phys.* **108**, 5319 (1998).
- <sup>24</sup>G. R. Low and H. G. Kjaergaard, *J. Chem. Phys.* **110**, 9104 (1999).
- <sup>25</sup>D. P. Schofield and H. G. Kjaergaard, *Phys. Chem. Chem. Phys.* **5**, 3100 (2003).
- <sup>26</sup>J. P. Perchard, *Chem. Phys.* **273**, 217 (2001).
- <sup>27</sup>J. P. Perchard, *Chem. Phys.* **266**, 109 (2001).
- <sup>28</sup>V. Vaida and J. E. Headrick, *J. Phys. Chem. A* **104**, 5401 (2000).
- <sup>29</sup>G. T. Evans and V. Vaida, *J. Chem. Phys.* **113**, 6652 (2000).
- <sup>30</sup>S. M. Kathmann, G. K. Schenter, and B. C. Garrett, *J. Chem. Phys.* **111**, 4688 (1999).
- <sup>31</sup>C. E. Kolb, J. T. Jayne, D. R. Worsnop, M. J. Molina, R. F. Meads, and A. A. Viggiano, *J. Am. Chem. Soc.* **116**, 10314 (1994).
- <sup>32</sup>A. B. Ryzhkov and P. A. Ariya, *Chem. Phys. Lett.* **367**, 423 (2002).
- <sup>33</sup>P. M. Pawlowski, S. R. Okimoto, and F.-M. Tao, *J. Phys. Chem. A* **107**, 5327 (2003).
- <sup>34</sup>L. E. Christensen, M. Okumura, S. P. Sander, R. J. Salawitch, G. C. Toon, B. Sen, J. F. Blavier, and K. W. Jucks, *Geophys. Res. Lett.* **29**, 13/1 (2002).
- <sup>35</sup>K. Pfeilsticker, A. Lotter, C. Peters, and H. Boesch, *Science* **300**, 2078 (2003).
- <sup>36</sup>R. L. Vanderwal, J. L. Scott, and F. F. Crim, *J. Chem. Phys.* **94**, 1859 (1991).
- <sup>37</sup>R. L. Vanderwal and F. F. Crim, *J. Phys. Chem.* **93**, 5331 (1989).
- <sup>38</sup>P. Andresen, V. Beushausen, D. Hausler, H. W. Lulf, and E. W. Rothe, *J. Chem. Phys.* **83**, 1429 (1985).
- <sup>39</sup>D. F. Plusquellic, O. Votava, and D. J. Nesbitt, *J. Chem. Phys.* **101**, 6356 (1994).
- <sup>40</sup>O. Votava, D. F. Plusquellic, T. L. Myers, and D. J. Nesbitt, *J. Chem. Phys.* **112**, 7449 (2000).
- <sup>41</sup>K. M. Christoffel and J. M. Bowman, *J. Chem. Phys.* **104**, 8348 (1996).
- <sup>42</sup>R. C. Cohen and R. J. Saykally, *J. Chem. Phys.* **98**, 6007 (1993).
- <sup>43</sup>S. A. Nizkorodov, M. Ziemkiewicz, T. L. Myers, and D. J. Nesbitt, *J. Chem. Phys.* **119**, 10158 (2003).
- <sup>44</sup>R. Schinck, R. L. Vanderwal, J. L. Scott, and F. F. Crim, *J. Chem. Phys.* **94**, 283 (1991).
- <sup>45</sup>M. S. Child and L. Halonen, *Adv. Chem. Phys.* **57**, 1 (1984).
- <sup>46</sup>R. C. Cohen and R. J. Saykally, *Annu. Rev. Phys. Chem.* **42**, 369 (1991).
- <sup>47</sup>D. J. Nesbitt and R. Lascola, *J. Chem. Phys.* **97**, 8096 (1992).
- <sup>48</sup>R. C. Cohen, K. L. Busarow, K. B. Laughlin, G. A. Blake, M. Havenith, Y. T. Lee, and R. J. Saykally, *J. Chem. Phys.* **89**, 4494 (1988).
- <sup>49</sup>L. B. Braly, J. D. Cruzan, K. Liu, R. S. Fellers, and R. J. Saykally, *J. Chem. Phys.* **112**, 10293 (2000).
- <sup>50</sup>L. H. Coudert, F. J. Lovas, R. D. Suenram, and J. T. Hougen, *J. Chem. Phys.* **87**, 6290 (1987).
- <sup>51</sup>V. Engel, V. Staemmler, R. L. Vanderwal *et al.*, *J. Phys. Chem.* **96**, 3201 (1992).
- <sup>52</sup>M. J. Weida and D. J. Nesbitt, *J. Chem. Phys.* **106**, 3078 (1997).
- <sup>53</sup>C. M. Lovejoy and D. J. Nesbitt, *J. Chem. Phys.* **91**, 2790 (1989).
- <sup>54</sup>M. Ziemkiewicz, C. Pluetzer, and D. J. Nesbitt (unpublished).
- <sup>55</sup>O. Votava, Ph.D. thesis, University of Colorado, 1999.
- <sup>56</sup>L. Oudejans and R. E. Miller, *J. Chem. Phys.* **113**, 4581 (2000).
- <sup>57</sup>L. Oudejans and R. E. Miller, *Annu. Rev. Phys. Chem.* **52**, 607 (2001).